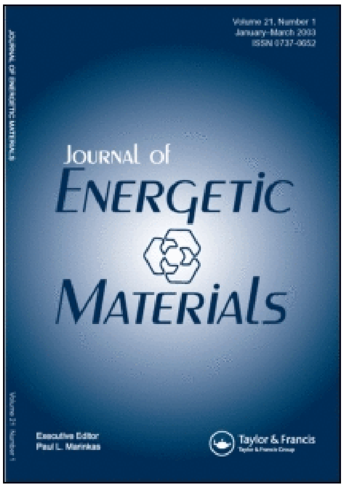

Journal of Energetic Materials
Publication details, including instructions for authors and subscription information:
http://www.informaworld.com/smpp/title~content=t713770432

Processing of Gun Propellants in Continuous Shear Roll Mills

Halil Gevgilili[a]; Dilhan M. Kalyon[a]; Anand Shah[a]
[a] Stevens Institute of Technology, Castle Point Station, Hoboken, New Jersey, USA

To cite this Article Gevgilili, Halil , Kalyon, Dilhan M. and Shah, Anand(2008) 'Processing of Gun Propellants in Continuous Shear Roll Mills', Journal of Energetic Materials, 26: 1, 29 — 51
To link to this Article: DOI: 10.1080/07370650701719196
URL: http://dx.doi.org/10.1080/07370650701719196

Journal of Energetic Materials, 26: 29–51, 2008

ISSN: 0737-0652 print/1545-8822 online
DOI: 10.1080/07370650701719196

Processing of Gun Propellants in Continuous Shear Roll Mills

HALIL GEVGILILI
DILHAN M. KALYON
ANAND SHAH

Stevens Institute of Technology, Castle Point Station, Hoboken, New Jersey, USA

The processing of gun propellants can be carried out using the continuous shear roll milling process, which consists of two counterrotating and grooved rolls that are run at different speeds and temperatures and that exhibit different surface roughnesses. During the shear roll milling process, the water content of the propellant is decreased upon heat transfer with the rolls and upon the viscous energy dissipation generated, especially when the propellant is subjected to the shearing action at the nip regions between the two rolls. The propellant can also be granulated. In this process the propellant needs to stick to one roll and detach from the surface of the second roll. Here a mathematical model of the process is developed and is used to explain the experimental findings collected during the shear roll milling of a live gun propellant formulation.

Keywords: mill, processing, propellant, shear roll

Introduction

Various roll-driven operations including calendering, roll milling, and continuous shear roll milling processes can be used for

Address correspondence to Dilhan M. Kalyon, Stevens Institute of Technology, Castle Point Station, Hoboken, NJ 07030, USA. E-mail: dkalyon@stevens.edu

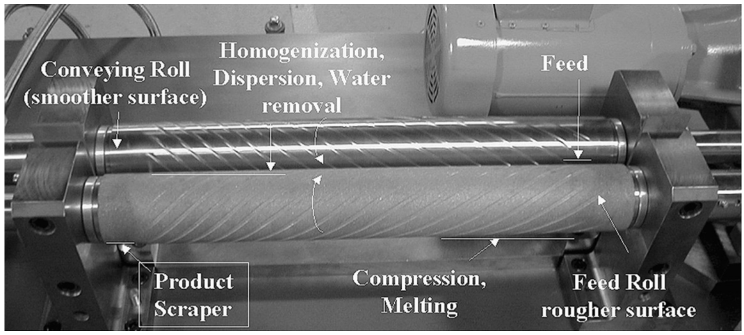

Figure 1. The basic features of the shear roll mill.

processing of propellants. In these processes the propellant is pressurized and forced into the nip region between two rolls rotating at the same or different speeds. The sticking of the melt to one or both rolls and the eventual detachment of the polymer melt from one or both rolls define the processability window of the propellant formulation in such processes. Among these roll-driven processes the continuous shear roll milling process [1–4] is especially useful for the processing of various types of propellants.

The shear roll extruder involves two heated counterrotating rolls with grooves built into them (Fig. 1). The rolls typically have different roughnesses and are run at different temperatures and/or rotational speeds. The fundamental steps of the processing operation of the propellant are

1. Conveying and compaction of the feed material;
2. the melting of the binder if a thermoplastic binder is used;
3. the squeezing out and the evaporation of the water;
4. the dispersion and homogenization of the felt;
5. cutting and granulation.

Experimental Equipment, Procedures, and Observations

Simulant Runs and the Understanding Gained

Two different types of shear roll milling equipment were used in the project. First, a pilot-scale shear roll mill was designed and built for the shear roll milling experiments (Fig. 1). This pilot-scale shear roll mill had two 75-mm rolls and they were powered by two separate electrical drives with motor ratings of 2 HP and that could rotate at different rotational speeds. This shear roll mill was used with simulants to understand the basic flow and heat transfer mechanisms of the process. In these experiments, inert polymeric pellets were fed into the gap between the two rolls using an Acrison gravimetric feeder. The front roll, or ''feed roll,'' has a rougher surface and the melt typically continuously adheres only to the feed roll as a result of its higher surface roughness for similar feed and conveying roll temperatures. In our experimental equipment the feed roll contained two heat transfer zones controlled by the circulation of a heat transfer medium; i.e., typically a thermostated silicone oil. The first zone is adjacent to the feed end and the second heat transfer zone is located adjacent to the scraper end, at which the polymer is removed from the shear roll mill. A higher temperature is generally used at the first temperature control zone in comparison to the second temperature control zone of the feed roll to give rise to the faster melting of the polymer and to initiate stick to the conveying roll surface. There is only one temperature control zone in the conveying roll.

Under typical operating conditions, the material wraps around the feed roll and is in contact with the second ''conveying'' roll at the nip region between the two rolls. Thus, under steady-state processing conditions, the melt typically periodically sticks and then detaches from the conveying roll every time it goes through the nip region, whereas the melt continuously sticks to the feed roll. Furthermore, the temperature of the feed roll is typically set higher than the temperature of the conveying roll. This guarantees the adhesion of material to feed roll.

When both roll temperatures are identical, the melt continuously sticks to only the feed roll. However, our experiments revealed that if the temperature of the conveying roll is set approximately 17°C higher then the feed roll, the melt sticks onto the conveying roll in spite of its smoother surface At slightly lower temperatures the process may become unstable and the melt can switch the roll onto which it continuously sticks.

Overall, a combination of the surface roughness and the temperature difference on the two rolls determines the roll onto which the melt continuously sticks.

The principal parameters of our experimental study were the rotational speeds of the feed and conveying rolls. The mass flow rate, the gap between the rolls, and the temperatures of the rolls were held constant (the two rolls were kept at the same temperature). An Inframetrics Thermacam PM 290 thermal imaging camera, manufactured by FLIR Systems of Boston, MA, was employed during these experiments to determine the surface temperature distribution of the rolls prior to the initiation of the extrusion process and the temperature distribution of the melt at its free surface as a function of location during the experiments. The thermal imaging camera has a working range of -10 to 450°C and an accuracy of ± 0.2°C. Thermonitor 95 Pro remote analysis software, available from FLIR Systems of Boston, MA, was used for the collection and analysis of the thermal images. The typical distribution of the temperature of the melt during the process indicates that the temperature of the melt is kept within a narrow range from the inlet to the exit of the shear roll milling process. The oil temperatures in the two rolls were set differently to achieve the reported roll surface temperatures. The emissivity values of the two surfaces were determined and were used in the temperature determination.

Upon reaching steady-state for each run (as evidenced by steady-state temperature distributions of the melt with the thermal imaging camera), we performed a pulse-input tracer residence time distribution experiment. For the pulse-incorporation of the tracer, we injected pulses consisting of a simulant with a carbon black tracer into the feed and recorded the progress of the color tracer using a digital video camera. The carbon black tracer did not spread significantly in the axial direction but rather formed relatively narrow rings, the width of which did not increase substantially in the axial direction, suggesting that the backmixing occurring in the shear roll mill is limited. Figure 2 shows the typical motion history of the melt during the shear roll milling process as

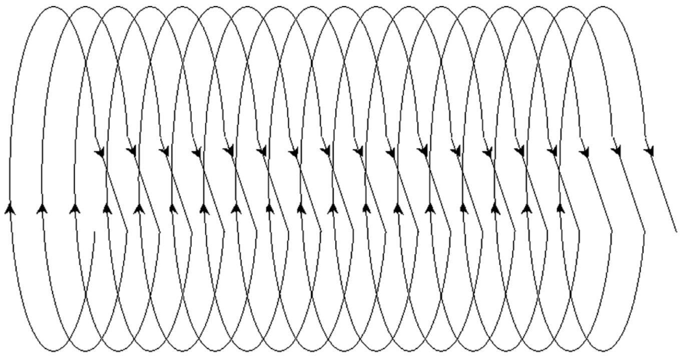

Figure 2. Path line of a particle on the feed roll.

deduced from these tracer experiments. Since there is no barrel, the shear roll mill conveys the material forward only through the intervention of the second roll. The nip region allows the material between the two rolls to be pressurized and conveyed, as if it were processed in a calender and followed by a whole revolution during which no further deformation takes place. Upon reaching the next nip region the material is once again deformed, pressurized, backmixed, generates new free surfaces, and is conveyed forward. On our 75-mm pilot-scale shear roll mill this corresponds to 200 passages through the nip region.

After the completion of various experiments, we simultaneously brought both rolls to a complete stop (‘‘dead stop’’) and measured the wall thickness of the film at ambient temperature and hence the weight distribution under steady flow or at the point that the unstable flow is initiated as evidenced through the detachment of the polymer melt from both rolls. The data suggest that the conveying capability of the shear roll mill changes with the operating conditions used. Typically, the increased roll speeds give rise to increased conveying capability as indicated by the reduced thickness of the material on the rolls and hence a reduced mean residence time during the process.

Processing of Live Gun Propellant

A second set of experiments was carried out using a shear roll mill with roll diameters of 200 mm in conjunction with a live gun propellant. The overall length of the rolls was around 130 cm and thus generates a length-over-diameter ratio of 130/20; i.e., 6.5. The rolls are heated in a multizone arrangement. The gap between the two rolls can theoretically be set, but as our experiments have shown in reality the gap cannot be controlled precisely. The propellant is fed into the gap between the two rolls. A container placed at the bottom indicated that some of the material does not stick to the rolls and falls immediately to the bottom. With the manufacturing scale shear roll mills, one of the rolls is polished (back) and the other is roughened (front). Both rolls have grooves built into them, with the helix angle of the grooves remaining constant from one end of the shear roll mill to the end. At the granulator end the grooves on the rolls run out and the propellant is forced to flow into a sieve followed by a cutter.

We have used two thermal cameras and two video cameras during the operation of the shear roll mill with the live propellant formulation. The thermal cameras were connected to two laptop computers. We have used remote control software for the collection of the thermal images as the experiments took place.

The live propellant felt on the back roll during the operation is shown in Figure 3. During the experiments with the live propellant it was determined that:

1. The propellant felt is not evenly distributed on the rolls. There seems to be a lot of material in the nip region, and the volume of material is the greatest at locations not directly at the feed zone but at the intermediary locations between the feed and the mid-point of the length of the shear roll mill.
2. The amount of material in the nip region appears to decrease with increasing distance in the down-channel direction.
3. The felt does not stick well to the roll surface in the feed section. The stick condition is generally observed as one moves in the down-channel direction.

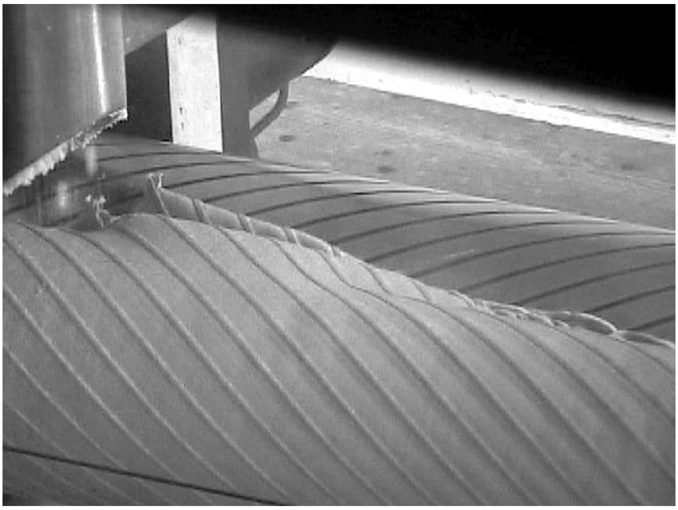

Figure 3. The live propellant felt on the back roll during the operation.

4. The felt only sticks to the front roll and not to the back roll.
5. There seems to be a lot of air encapsulated in the felt especially in the nip region, where the felt is pleated and folds back on itself repeatedly (see Fig. 4).
6. The felt initially does not stick well to the surface of the roll.
7. There are pockets of water vapor, which can be seen from the deformation of the felt surface. This should be a result of the vaporization of the water at the surface of the rolls and its encapsulation by the presence of the felt and the lack of a mechanism for the diffusion of the water vapor out of the felt (limited by the solubility of the water vapor in the felt).
8. The felt is compressed at the nip region with pockets of air also squeezed (see Figs. 3, 4). This may generate an adiabatic compression problem if the air pocket is squeezed relatively fast and the air pocket is relatively large with no pathway for the air to escape. It is also

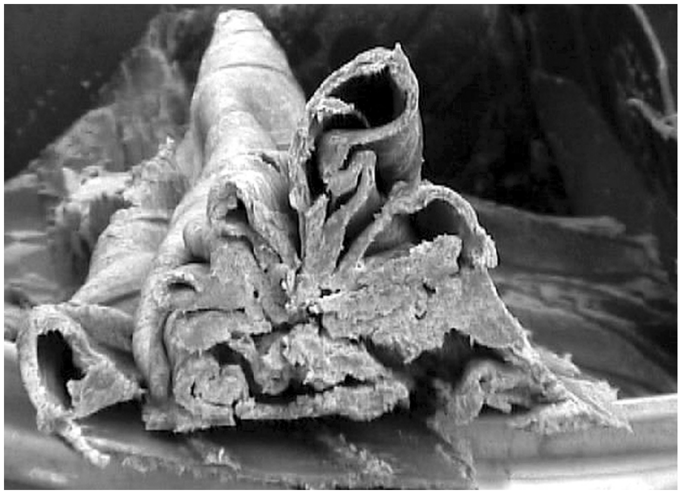

Figure 4. Air is encapsulated in the felt especially in the nip region, where the felt is pleated and folds back on itself repeatedly.

seen how difficult it is for the felt to be squeezed in the nip region, suggesting that significant forces need to be applied for the gun propellant to be forced into the nip area.

9. The forward motion of the felt is controlled by the deformation occurring at the nip.
10. The roughness of the rolls and the roll temperatures are important because they control the slip/stick behavior of the felt on the rolls.
11. Without the sticking of the material onto the rolls there is no mechanism for forward motion and the generation of viscous energy dissipation on a material that is not moving forward will lead to rapid moisture loss and the burning of the propellant.

During the live runs, the screw rotational speeds could be kept at the targeted values. The typical roll speeds were 42 rpm for the front and 35 rpm for the back roll. This difference in the screw speeds is another important aspect of the shear roll mill process. The front roll (which holds the felt) generally is

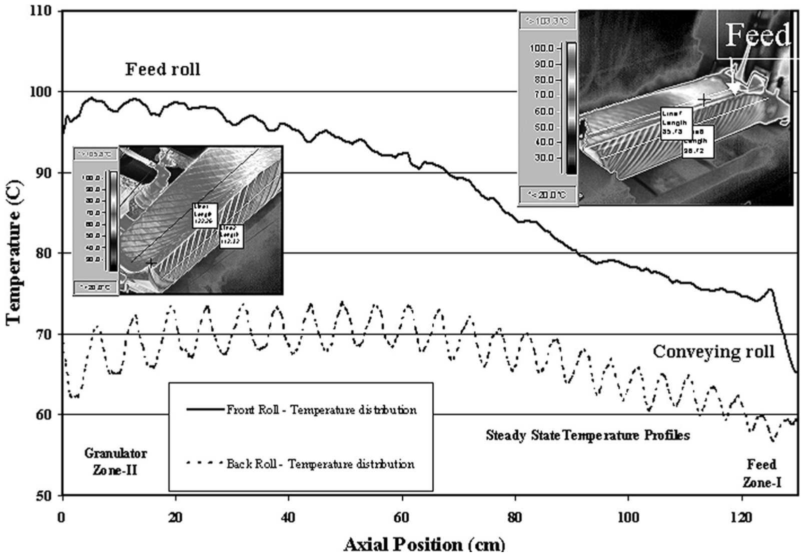

Figure 5. Typical roll temperature profiles prior to a run.

rotated at a faster speed than the back roll, which is used to pressurize and move the material in the forward direction. On the other hand, the temperature of the front roll is always greater than the back roll. This again makes sense since the felt should stick to the hotter surface and slip away from the colder surface. There is a significant difference (over 20°C) between the temperatures on the feed roll and the surface temperatures of the conveying roll (Fig. 5). The torques on the front and the back rolls were also measured and suggested that the torque on the front roll was greater than on the back roll. The initial and the product moisture levels and the product density values were also determined. Figure 5 also indicates that following the settings the feed end of the rolls are at a greater temperature in comparison to the granulator (exit) end of the shear roll mill. During the run the temperature of the propellant felt increases asymptotically with time. The rate of change of temperature with time is relatively high at the beginning of the run but slows down sufficiently so that a steady state can be assumed after 10–15 min of operation (Fig. 5 provides the steady-state condition). The temperature of the felt increases from the feed section to the granulation section of the rolls. Furthermore, the temperature distribution results indicate that the surface temperatures of the rolls are less than the set values at the beginning of the runs.

The determination of the propellant felt thickness distribution indicates that the felt thickness is dependent on the gap setting used in the run but is not even close to the initial gap thickness. For example, a gap setting of 0.5 mm generates felt thicknesses of 1.61 to 2.25 mm. Thus, the felt thickness is controlled by other mechanisms, the most likely of which is the separation of the two rolls under the force generated by the squeezing of the felt into the nip region. Overall, the greater initial gap separation also gives rise to an increased felt thickness. A complete set of tracer incorporation and residence time distribution determination upon pulse type tracer input were also carried out on the live propellant. These results indicated that consistent with the findings of the simulant runs on the prototype shear roll mill, the residence time distribution is narrow, indicating that the propellant is translated with very little intermixing in between the different channels formed by the presence of the grooves (see Fig. 1).

Process Analysis: Mathematical Modeling of the Shear Roll Mill Process Using 1-D Model and Macroscopic Energy Balance

It is possible to carry out the numerical analysis of the flow dynamics especially using FEM [5–11] but an analytical analysis using the lubrication flow assumption is preferable at the outset to better understand the relationship between various parameters and their effects on the thermo-mechanical history that is generated during the process. The analysis of the shear roll mill process can be simplified considerably if the forward motion of the material in a shear roll extruder is neglected. This is generally justified because the forward velocities of the melt are a couple of orders of magnitude smaller than the roll velocities

It is the interface between the two rolls, which translates the felt in the forward direction and generates the compression and the pressurization of the felt, and the squeezing out of its water. The nip area also allows some degree of backmixing, during which the material is circulated and new free surface is generated, allowing the water vapor to be released to the environment. Overall, only heat transfer is important during the travel of the felt from one nip region to the other. The velocity distribution is known (identical to the radial velocity of the feed roll) and is flat at the point that the felt is detached from the rolls. The velocity distribution changes significantly as a function of distance in the down-channel direction when the felt is in between the two rolls.

The model that will be used here is based on the general treatise of Gaskell and McKelvey [12–17]. In this analysis the flow is assumed to be laminar, incompressible, quasi-isothermal, and laminar. The rolls have a radius of R and rotate in opposite directions with frequency of rotation of N. The minimum nip separation is H_0 and the material is distributed laterally over a distance of W, which spans the distance from $x = X_2$, where the rolls bite into the material upstream to $x = X_1$, where the material detaches from the conveying roll downstream, $x = 0$ being the point of minimum gap separation. Hence, W is equal to sum of X_1 and X_2. The pressure is atmospheric at X_1 and X_2. The ratio of the distance of separation between the rolls to radius H/R is assumed to be small, which enables us to assume that the velocity profile at any location x is considered identical to the velocity profile between two parallel plates, which are 2 h distance apart. The equations of continuity and momentum will reduce to:

$$\frac{dv_x}{dx} = 0 \tag{1}$$

$$\frac{\partial P}{\partial x} = \frac{\partial \tau_{yx}}{\partial y} = \mu \frac{\partial^2 v_x}{\partial y^2} \tag{2}$$

with the boundary conditions, $v_x(\pm h) = U$, where U is the tangential velocity of the roll surfaces, $U = 2\Pi NR$ and $\pm h$

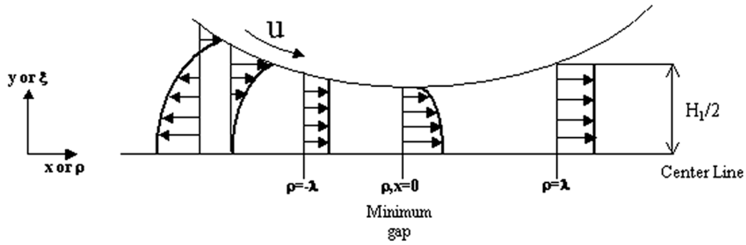

Figure 6. Schematic drawing of the nip region of the shear roll mill and the velocity profiles for similar roll speeds.

correspond to the two roll surfaces. The distance 2 h between the two rolls changes in the nip as the material travels down stream. The functional relationship between h and x at any downstream location between X_1 and X_2 is (Fig. 6):

$$h = H_0 + R - \sqrt{R^2 - x^2} \tag{3}$$

The momentum equation can be rearranged to

$$\frac{dP}{dx} = \frac{3\mu U}{H_1^2}\left(1 - \frac{H_1}{h}\right)\left(\frac{H_1}{h}\right)^2 \tag{4}$$

where h equals to H_1 at $x = X_1$. This equation implies that the pressure gradient is zero at X_1, at the detachment point, where the pressure drops to atmospheric pressure and at X_1, somewhere upstream form the minimum gap separation point, where the pressure attains a maximum.

Using binomial expansion, Eq. (3) can be approximated to

$$\rho^2 = \frac{x^2}{2RH_0} \tag{5}$$

At $x = X_1$ and $-X_1$; i.e., at the detachment and maximum pressure points

$$\lambda^2 = \frac{X_1^2}{2RH_0} \tag{6}$$

With these definitions and approximations it is possible to integrate Eq. (4) to the following form

$$P=\frac{3\mu U}{4H_0}\sqrt{\frac{R}{2H_0}}\left\{\left[\frac{\rho^2-1-5\lambda^2-3\lambda^2\rho^2}{(1+\rho^2)^2}\right]\rho+(1-3\lambda^2)\tan^{-1}\rho+C(\lambda)\right\} \tag{7}$$

with the integration constant being

$$C(\lambda)=\frac{(1+3\lambda^2)}{(1+\lambda^2)}\lambda-(1-3\lambda^2)\tan^{-1}\lambda \tag{8}$$

Similarly, starting from the continuity equation it is possible to obtain the velocity profile as:

$$u_x=1+\frac{3}{2}\frac{(1-\xi^2)(\lambda^2-\rho^2)}{(1+\rho^2)} \tag{9}$$

where u_x is the velocity normalized with respect to the roll velocity; i.e., v_x/U and ξ is the dimensionless gap y/H. Finally, knowing the velocity profile it possible to get the shear rate distribution as:

$$\dot{\gamma}_{yx}(\xi)=\frac{3U}{H_0}\frac{(\rho^2-\lambda^2)}{(1+\rho^2)^2}\xi \tag{10}$$

Using this relationship one can evaluate the viscous energy dissipation term within the nip, which needs to be utilized in the macroscopic energy balance (Fig. 7). The typical velocity and shear rate profiles in the nip region which were calculated using the 1-D calendering equations are shown in Figures 8 and 9. The negative velocity is indicative of the backmixing to occur at the entrance to the nip region. It should be noted that the Newtonian fluid assumption is a significant limitation since it is known that the shear viscosity of the felt, η, is not a constant but a material function which will vary as:

$$\eta=f(\text{shear rate, temperature, water concentration, degree of homogenization of the felt})$$

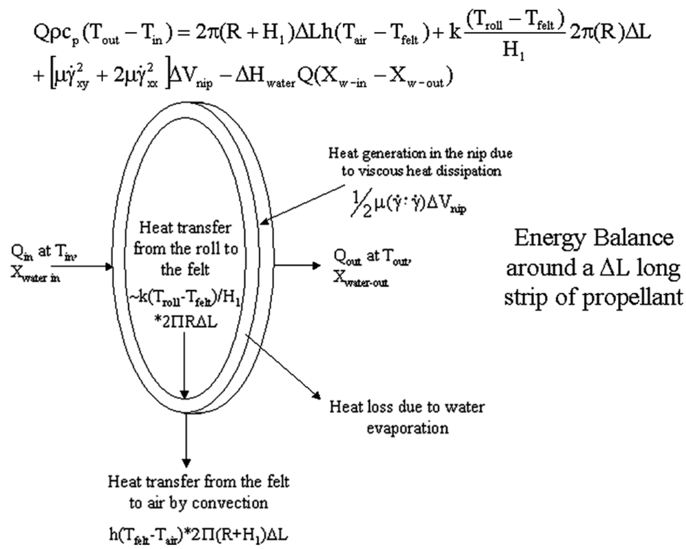

Figure 7. Macroscopic energy balance on a strip of material.

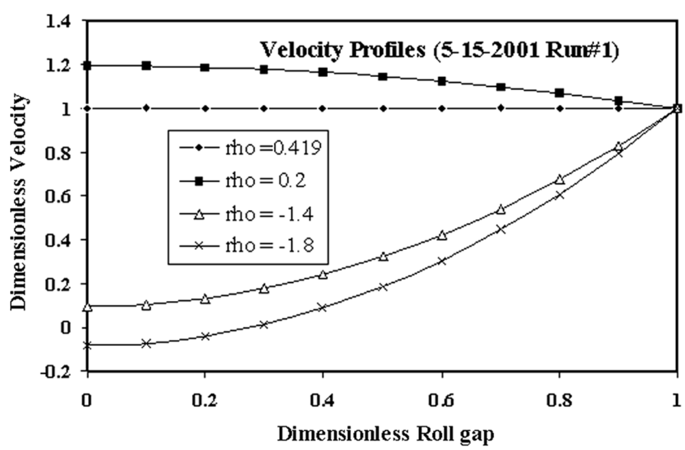

Figure 8. Dimensionless velocity profile of the material at various points along the nip.

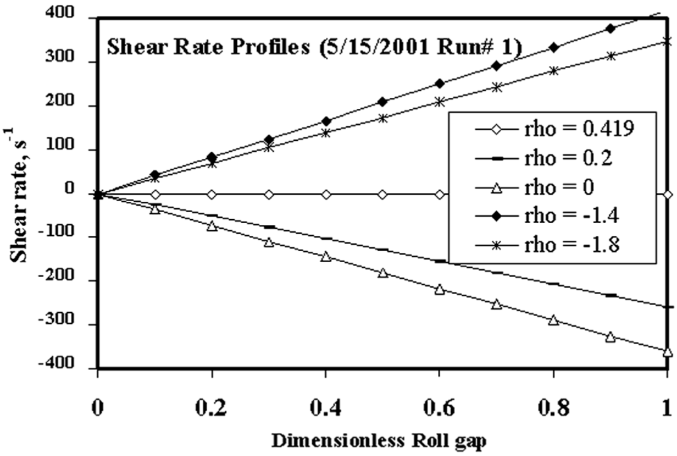

Figure 9. Shear rate profile within the nip.

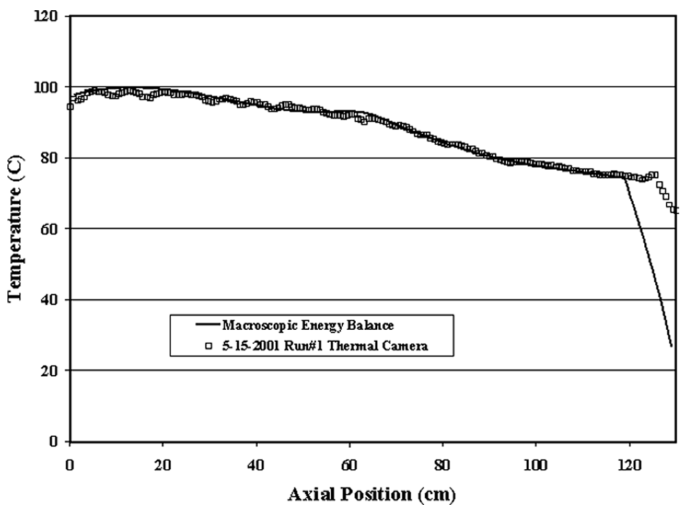

Figure 10. Experimental and predicted temperature profile along the rolls under following conditions: Flow rate = 45 kg/h, feed roll speed = 45 rpm, conveying roll speed 38 rpm, set temperature of the roll at the inlet section of the feed roll = 120°C, set temperature of the roll at the discharge section of the feed roll = 105°C, set temperature of the roll at the conveying roll = 90°C.

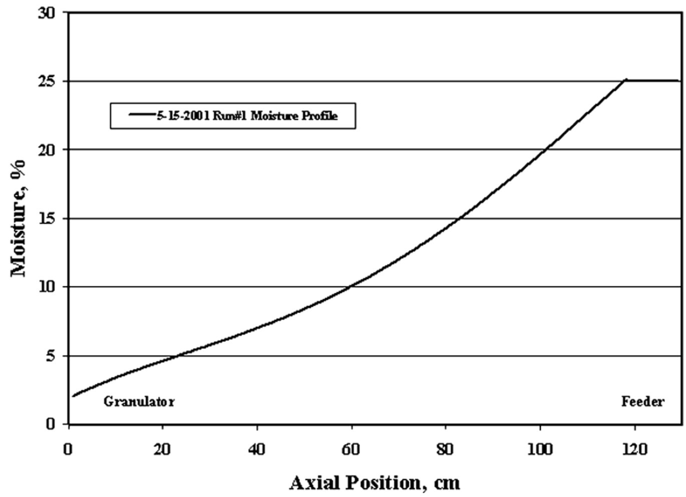

Figure 11. Predicted moisture level along the rolls under following conditions: Flow rate = 45 kg/h, feed roll speed = 45 rpm, conveying roll speed 38 rpm, set temperature of the roll at the inlet section of the feed roll = 120°C, set temperature of the roll at the discharge section of the feed roll = 105°C, set temperature of the roll at the conveying roll = 90°C.

Under the scope of this study, it was not possible for us to characterize the shear viscosity material function of the felt as a function of temperature, shear rate, water, and degree of homogenization. The macroscopic energy balance over a ring of felt is shown in Figure 7:

$$\begin{aligned}
&Q\rho c_p(T_{out}-T_{in})=2\pi(R+H_1)\Delta L h(T_{air}-T_{felt})\\
&+k\frac{(T_{roll}-T_{felt})}{H_1}2\pi R\Delta L\\
&+[\mu\dot{\gamma}_{xy}^2+2\mu\dot{\gamma}_{xx}^2]\Delta V_{nip}-\Delta H_{water}Q(X_{w-in}-X_{w-out}) \qquad (11)
\end{aligned}$$

The term on the left-hand side of the equation is the energy accumulation term representing the temperature change. The first term on the right-hand side is energy transferred from

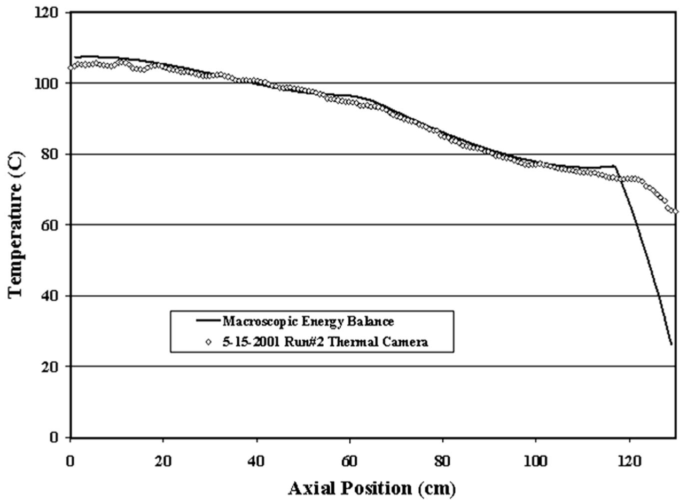

Figure 12. Experimental and predicted temperature profile along the rolls under following conditions: Flow rate = 40 kg/h, feed roll speed = 45 rpm, conveying roll speed 38 rpm, set temperature of the roll at the inlet section of the feed roll = 120°C, set temperature of the roll at the discharge section of the feed roll = 105°C, set temperature of the roll at the conveying roll = 90°C.

the felt to the surrounding air by free or forced convection, the second term represents the heat conduction from the roll surface to the felt, the third term stands for the viscous energy dissipation upon shearing and extension in the nip region, and the last term accounts for the heat loss due to water evaporation. The volume of propellant found in the nip region is designated by ΔV_{nip}.

The macroscopic energy balance is integrated by finite differences method. The thickness of the control volume (which is depicted in Figure 7 and over which the macroscopic balance was performed) was reduced gradually, until the results were independent of the density of the finite difference grid.

It is clear that the amount of water loss rate distributions are unknowns since this will depend on the exact mechanisms of evaporation upon the generation of the free surfaces in the

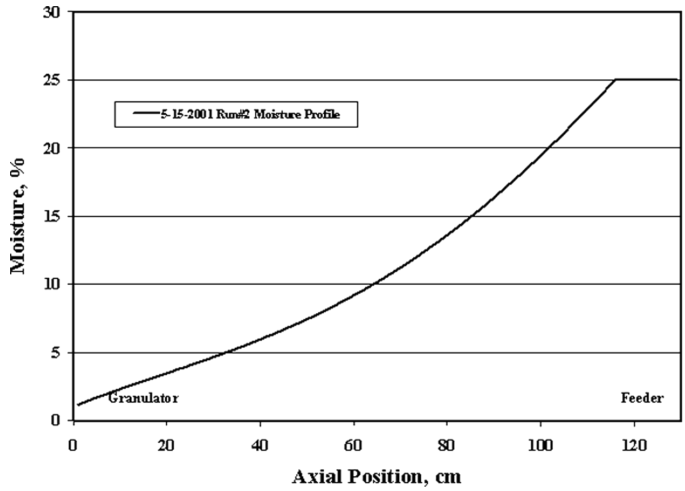

Figure 13. Predicted moisture level along the rolls under following conditions: Flow rate = 50 kg/h, feed roll speed = 45 rpm, conveying roll speed 38 rpm, set temperature of the roll at the inlet section of the feed roll = 120°C, set temperature of the roll at the discharge section of the feed roll = 105°C, set temperature of the roll at the conveying roll = 90°C.

nip region and diffusion of the water through the felt, the solubility of water in the components of the felt, etc. Thus, overall, there are two unknowns in the balance, one is the shear viscosity of the felt as a function of position, specific energy input history (the structure and hence the rheological behavior of the propellant should depend on the thermo-mechanical history that the propellant undergoes), and the amount of water lost. However, the concentration of the water in the feed and also the concentration of the water in the granules were known. The shear rate and the extension rates could be determined by the 1-D analysis.

The comparison of the temperature of the felt that is measured and fitted using the macroscopic balance and keeping the moisture loss rate and the shear viscosity of the felt as adjustable parameters are shown in Figures 10, 12, and 14. The corresponding losses of water as a function of distance in the shear

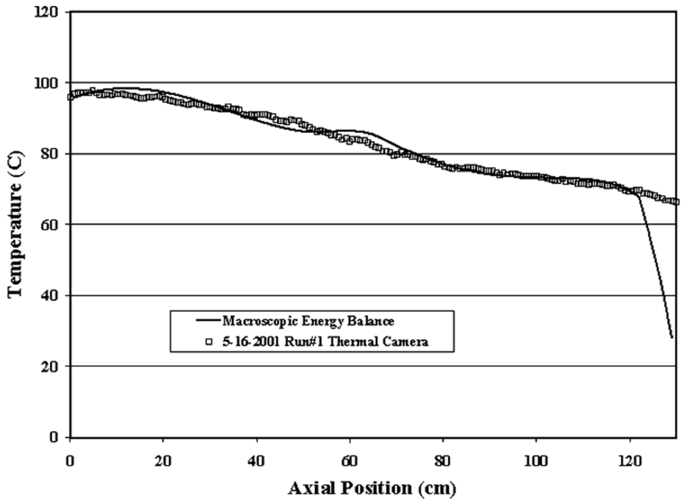

Figure 14. Experimental and predicted temperature profile along the rolls under following conditions: Flow rate = 40 kg/h, feed roll speed = 45 rpm, conveying roll speed 38 rpm, set temperature of the roll at the inlet section of the feed roll = 120°C, set temperature of the roll at the discharge section of the feed roll = 105°C, set temperature of the roll at the conveying roll = 90°C.

roll mill are also shown (Figs. 11, 13, 15). The fits are very reasonable, suggesting that the overall mechanisms assumed are relevant since a few adjustable parameters are sufficient to represent the entire behavior of the felt from the feed to the granulation sections. The only mismatch occurs in the hopper area. It is likely that some stagnant amount of propellant discovered during the tracer experiments is responsible for the noted discrepancy. The rate of water loss is initially high and decreases as the concentration of the water is reduced.

The variation of the water content with temperature is shown in Figure 16. The water concentration decreases with increasing average material temperature. The corresponding behavior of the shear viscosity of the gun propellant changing with the moisture content is shown in Figure 17. The shear

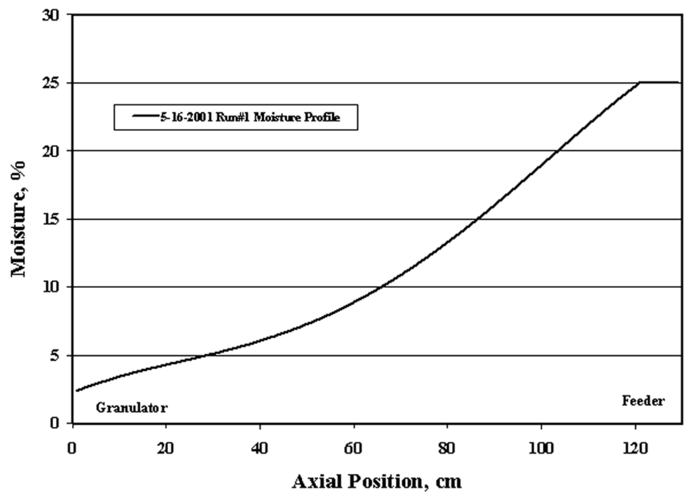

Figure 15. Predicted moisture level along the rolls under following conditions: Flow rate = 50 kg/h, feed roll speed = 45 rpm, conveying roll speed 38 rpm, set temperature of the roll at the inlet section of the feed roll = 120°C, set temperature of the roll at the discharge section of the feed roll = 105°C, set temperature of the roll at the conveying roll = 90°C.

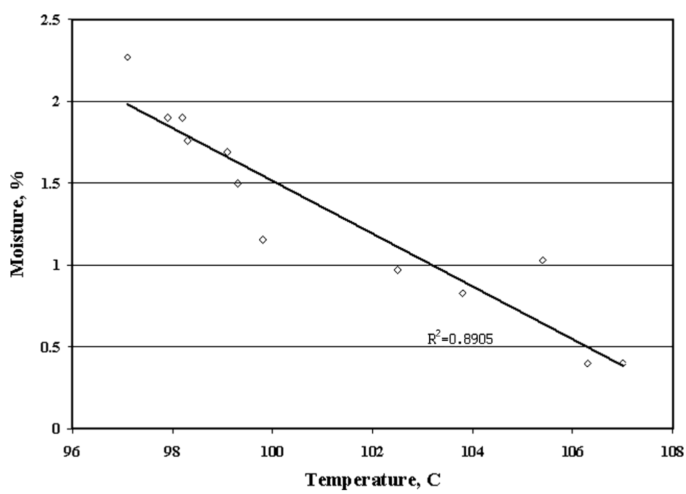

Figure 16. Correlation between the final moisture of the propellant and discharge temperature.

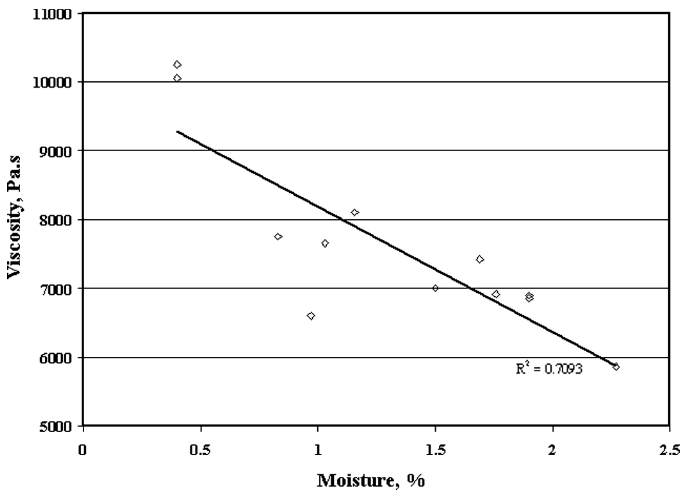

Figure 17. Correlation between the shear viscosity of the propellant and moisture content.

viscosity decreases with increasing water content. The shear viscosity value of the felt is around 7,000–10,000 Pa-s.

Conclusion

A mathematical model of the continuous shear roll milling of propellants is developed and elucidated under the light of experiments carried out upon processing of simulants and live gun propellants in continuous shear roll mills at various rates. The experiments included thermal imaging of the shear roll surfaces and the free surfaces of the propellant felt, and the thickness and the water concentration distributions of the propellant felt under differing processing conditions. Coupled with our previously published analysis of wall slip in continuous shear roll milling process [18], this analysis provides a first order undrestanding of the dynamics of the shear roll milling process to enable safer processing of gun propellants in continuous shear roll mills.

Acknowledgements

This work was supported by TACOM/ARDEC of Picattiny Arsenal, NJ, under contract DAAE30-01-C-1039. We are grateful for this support. We acknowledge with gratitude the contributions of Mr. James E. Kowalczyk and Mr. James B. Graybill of MPR Inc. of Hackensack, New Jersey, in the design and the manufacturing of the shear roll mill used in the experimental study. We also thank M. Malik, H. Tang, T. Kiryaman, and H. Filiz of Stevens; and C. Topolski, S. Rosenberg, D. Fair, A. Perich, W. Miller, N. Campesi, and E. Krajkowski of ARDEC at Picattiny Arsenal, Dr. Hays Zeigler of ATK Systems of Radford, Virginia; and Dr. A. Wellm of NitroChemie, Germany. We further thank the staff of NitroChemie for the diligent help they provided to our experimental program.

References

[1] Menges, G. and E. Krueger. 1985. Compounding of PVC. *Kunststoffe*, 75(5): 258–263.

[2] Berghaus, U., T. Bartilla, P. Heidemeyer, and G. Crolla. 1988. Polymerisation und blendherstellung, teil 3: Kontinuierliches mischen von polyvinylchlorid [Polymers and blends. Part 3: Continuous mixing of polyvinyl chloride]. *Plastverarbeiter*, 39: 70–72.

[3] Albers, A. 1992. Compounding with a shear roll extruder a new process for plastication and dispersion of highly viscous materials. *Kunststoffe*, 82(10): 982–987.

[4] Albers, A. 1994. Aufbereitung von Galvanik-und Lackschlaemmen mit kontinuierlichem *Scherwalzentrockner. Galvanotechnik*, 85(6): 1971–1973.

[5] Kiparissides, C. and J. Vlachopoulos. 1976. Finite element analysis of calendering. *Polymer Engineering and Science*, 16, 712–719.

[6] Kiparissides, C. and J. Vlachopoulos. 1978. Study of viscous dissipation in the calendaring of power-law fluids. *Polymer Engineering and Science*, 18: 210–214.

[7] Levine, L., C. M. Corvalan, O. H. Campanella, and M. R. Okos. 2002. A model describing the two-dimensional calendering of finite width sheets. *Chemical Engineering Science*, 57: 643–650.

[8] Klostermann, R., S. Von Bose, and D. Mewes. 1994. Comparison of calculated with measured flow fields in the gap between two rotating rolls. *Advances in Polymer Technology*, 13: 187–199.

[9] Agassant, J. F. and M. Espy. 1985. Theoretical and experimental study of the molten polymer flow in the calender bank. *Polymer Engineering and Science*, 25: 118–121.

[10] Ng, T. S. and G. Angerer. 1980. Estimation of the shear deformation exerted by a roll-mill upon a rubber compound. *Polymer Engineering and Science*, 20(8): 585–588.

[11] Yao, C. H. and I. Manas-Zloczower. 1996. Study of mixing efficiency in roll-mills. *Polymer Engineering and Science*, 36(3): 305–310.

[12] McKelvey, J. 1962. *Polymer Processing*. New York: John Wiley & Sons, 211–222.

[13] Middleman, S. 1977. *Fundamentals of Polymer Processing*. New York: McGraw Hill, 170–183.

[14] Tadmor, Z. and C. Gogos. 1979. *Principles of Polymer Processing*. New York: John Wiley & Sons, 661–682.

[15] Gaskell, R. 1950. The calendering of plastic materials. *Journal of Applied Mechanics*, 17: 334–341.

[16] Allston, W. and K. Astill. 1973. An analysis for the calendering of non-Newtonian fluids. *Journal of Applied Polymer Science*, 17: 3157–3174.

[17] Brazinsky, I., H. F. Cosway, C. F. Valle, and R. C. Jones. 1970. A theoretical study of liquid-film spread heights in the calendering of Newtonian and power law fluids. *Journal of Applied Polymer Science*, 14(11): 2771–2784.

[18] Kalyon, D., H. Gevgilili, and A. Shah. 2004. Detachment of the polymer melt from the roll surface: Data from a shear roll extruder. *International Polymer Processing*, 19(2): 129–138.